-Supporting Information-

Solution Growth of Ultralong Gold Nanohelices

Yong Wang,[‡§], Jiating He,[§] Xiaoke Mu,[||] Di Wang,[||] Bowei Zhang,[⊥] Youde Shen,[#] Ming Lin,[§] Christian Kübel,[||] Yizhong Huang,[⊥] and Hongyu Chen*[,†‡]

[†]Institute of Advanced Synthesis (IAS), School of Chemistry and Molecular Engineering, Jiangsu National Synergetic Innovation Centre for Advanced Materials, Nanjing Tech University, Nanjing 211816, P. R. China. E-mail: iashychen@njtech.edu.cn

[‡]Division of Chemistry and Biological Chemistry, School of Physical and Mathematical Sciences, Nanyang Technological University, Singapore 637371

[§]Institute of Materials Research and Engineering, A*STAR (Agency for Science, Technology and Research), #08-03, 2 Fusionopolis Way, Innovis, 138634, Singapore.

[||]Institute of Nanotechnology and Karlsruhe Nano Micro Facility, Karlsruhe Institute of Technology, Karlsruhe, 76021, Germany.

[⊥]School of Materials Science and Engineering, Nanyang Technological University, 639798, Singapore.

[#]Division of Physics and Applied Physics, School of Physical and Mathematical Sciences, Nanyang Technological University, 637371, Singapore.

E-mail: iashychen@njtech.edu.cn; hongyuchen@ntu.edu.sg

Discussion about the floccules

We have carried out the following experiments to understand the nature of the "floccule". In the synthesis, there are several reactants and solvents: ligand, ascorbic acid, $HAuCl_4$, and the mixed solvent (ethanol and water).

1) Study the minimal conditions of forming the floccules. This part has already been discussed in the manuscript. Ethanol was present to assist the initial solubilization of the ligand **1**. Basically, without ligand there is no floccules; Au(III) does not form floccules while the reduced Au(I) can. Hence, it appears that the floccules are made of Au(I) complex of the ligand **1**, and the white color is also consistent with Au(I) complex.
2) Test the solubility of the ligand versus the floccules. The ligand **1** is soluble in ethanol, CH_2Cl_2, and other polar organic solvent. The floccules are not soluble in water, in neat organic solvents (ethanol, DMSO, DMF, CH_2Cl_2, etc.) and nor in base solutions (2 M). In 2 M NaOH solution with elevated temperature (60 °C), the floccules dissolve, likely due to the hydrolysis of the ester group.
3) Redox chemistry of the floccules. After growth of helices, addition of $NaBH_4$ in the remaining floccules gave a dark brown color solution with simultaneous dissolution of most of the floccules. As shown in the images below, TEM characterization showed numerous Au nanoparticles of 5-10 nm in diameter (hence the dark brown color). The sudden appearance of these Au nanoparticles suggests that Au exists at a higher oxidation state than 0 in the floccules.

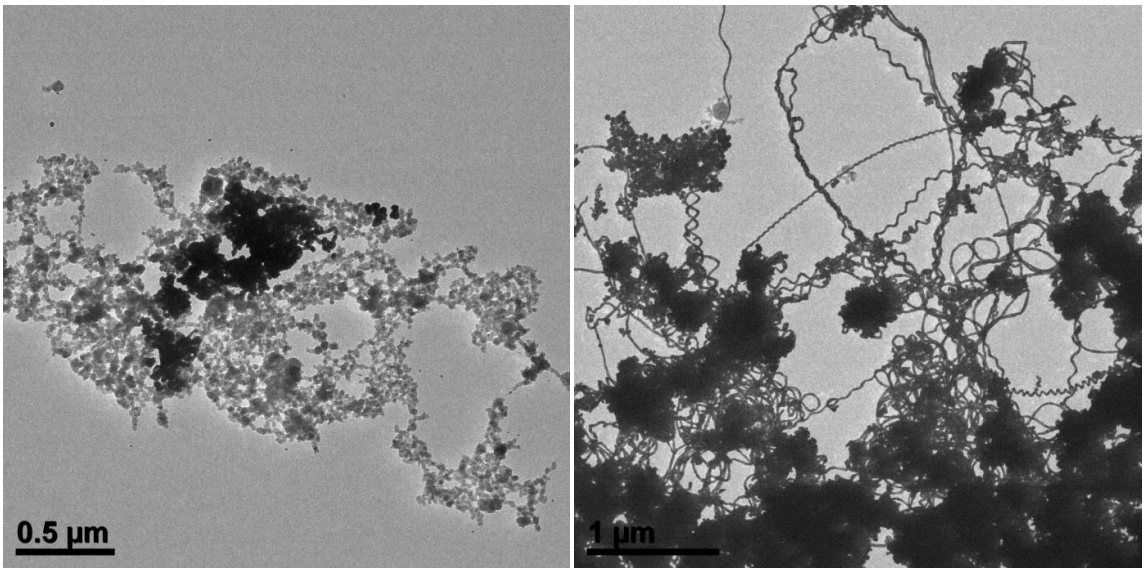

Figure S1. TEM images of the product by adding $NaBH_4$ in the solution after growth of helices for 24 h.

4) *In situ* TEM. As shown in *Figure S27,* the floccules were isolated by centrifugation for TEM investigation. Once focused at a small area (*i.e.*, with large dose of electron beam applied), the fiber-like floccules change to arrays of small nanoparticles, consistent with the reduction of the Au(I) species.

5) FT-IR. The FT-IR spectra of the ligand **1** and the floccules are shown below. The peaks between 470 and 530 cm^{-1} can be assigned to the S-S stretching (Biomedicine & Pharmacotherapy 65 (2011) 334-338). Their intensity decreases dramatically from the pure ligand **1** to the floccules, consistent with thiolate formation and coordination to Au.

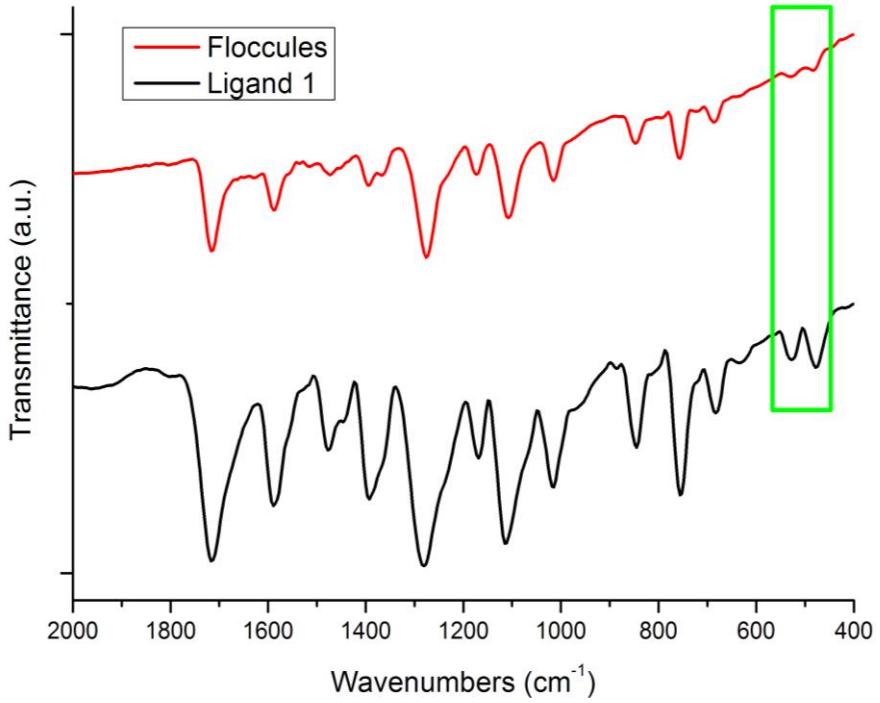

Figure S2. FT-IR spectra of the ligand 1 and the floccules.

6) XRD. We also measured XRD of various materials for comparison: the ligand **1**, floccules (about 5 hours after the mixing of reactants), and commercially available Au(I)Cl complex. It is clear that the peaks of ligand **1** disappeared in floccules, suggesting the formation of complexes. The floccules show two broad and weak peaks around 38º and 65º, which are consistent with the (111) and (220) peaks of Au, likely because of small Au(0) particles at this reaction time.

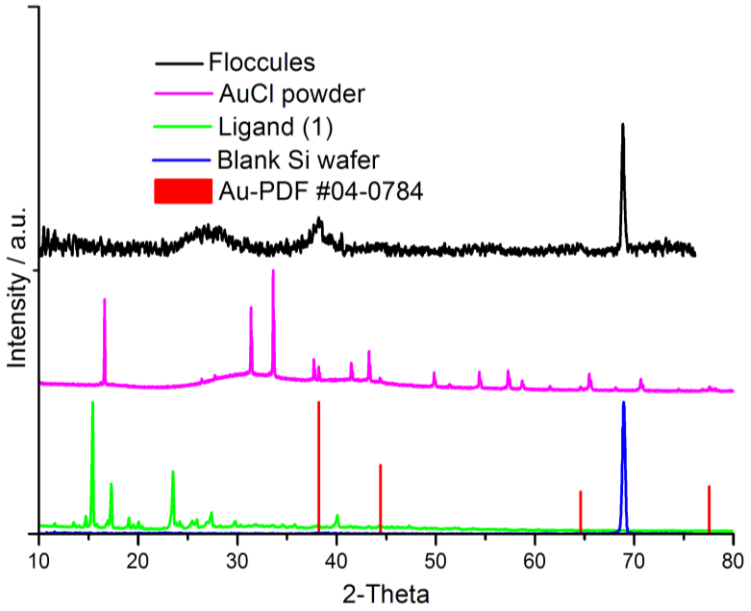

Figure S3. XRD patterns of various materials for comparison.

7) XPS. The X-ray photoelectron spectroscopy (XPS) of the floccules (about 5 h after mixing of reactants) has also been measured. The curve fitting below shows that the dominant species of Au in the floccules is Au(I), with a minor contribution from Au(III).

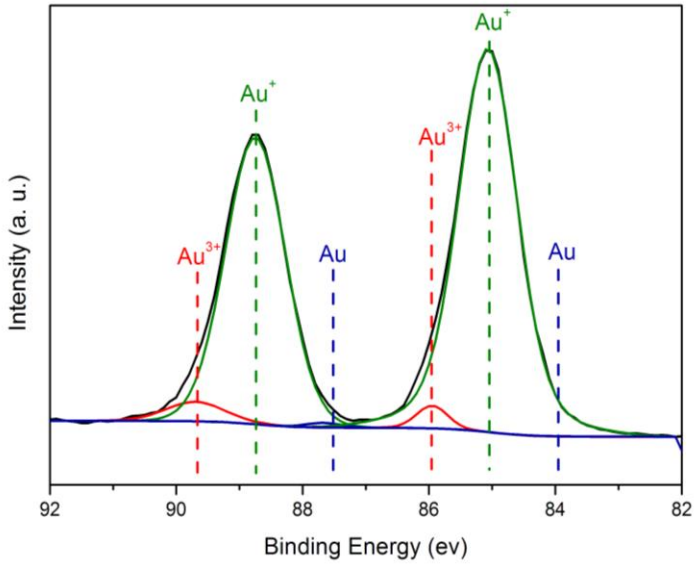

Figure S4. X-ray photoelectron spectroscopy (XPS) of the floccules (about 5 h after mixing of reactants).

Hence, all of the evidences above support the formation of complex from Au(I) and ligand **1** in the floccules.

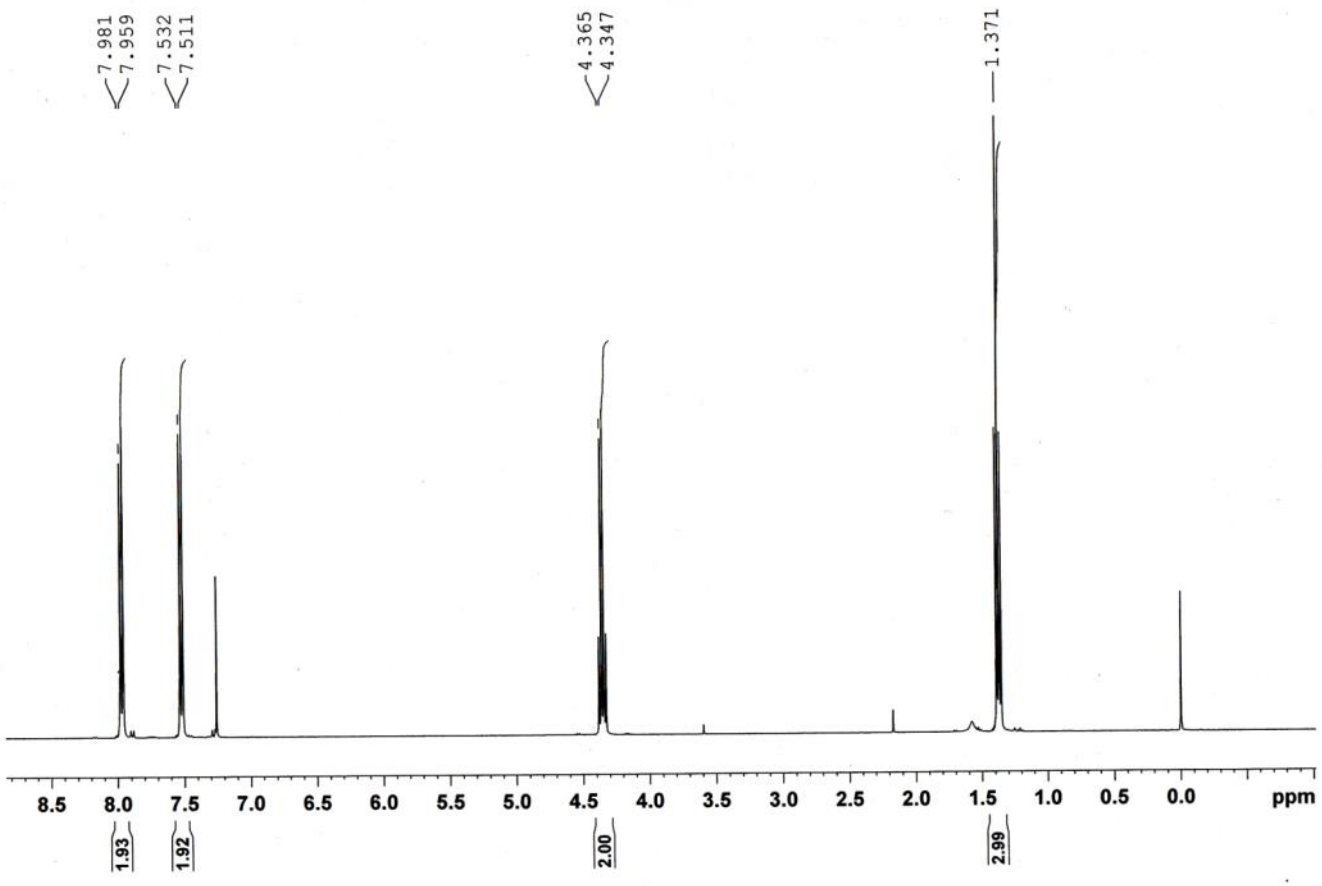

Figure S5. NMR spectrum of the as-synthesized **1.**

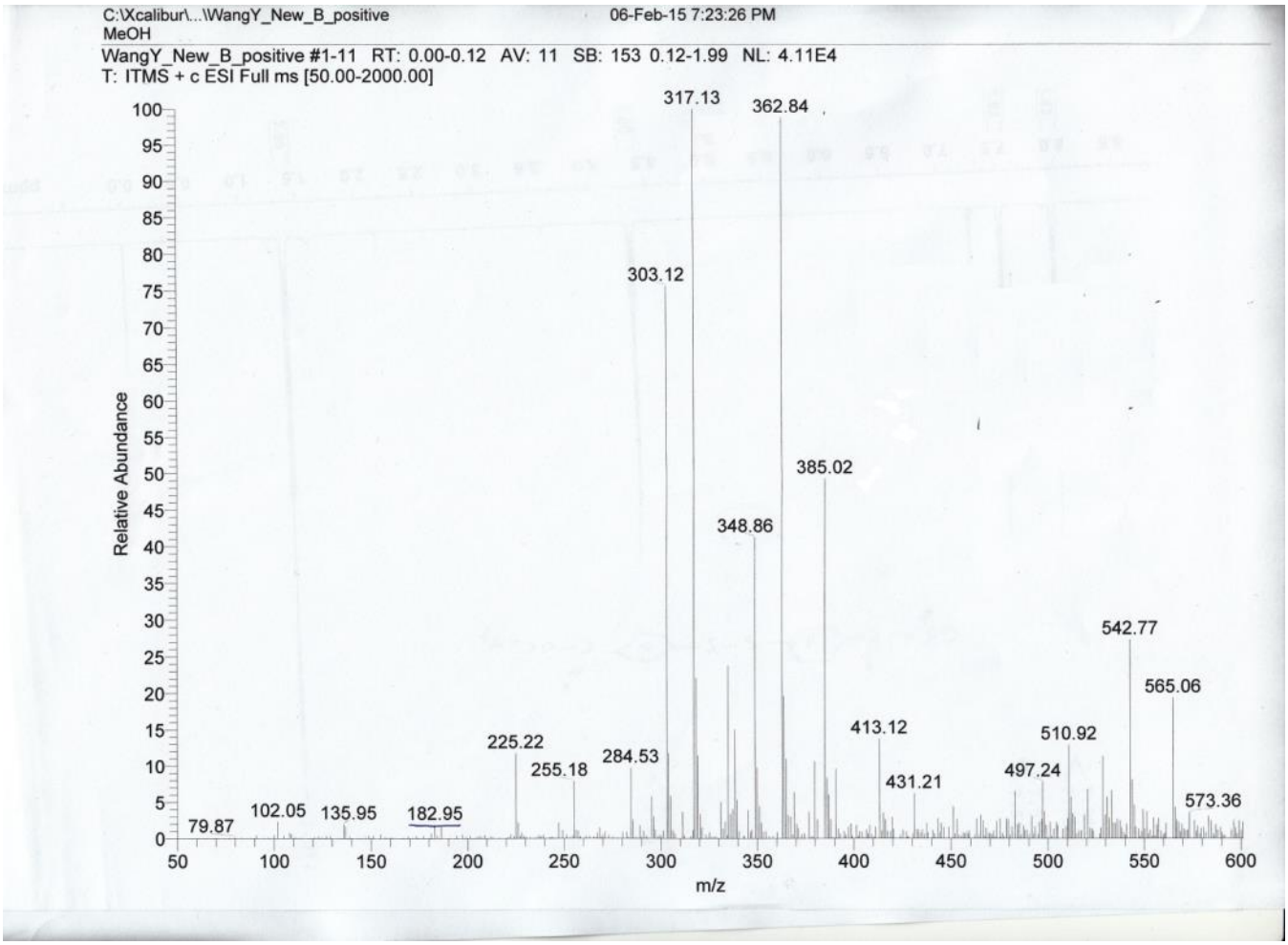

Figure S6. ESI-MS analysis of the as synthesized **1.**

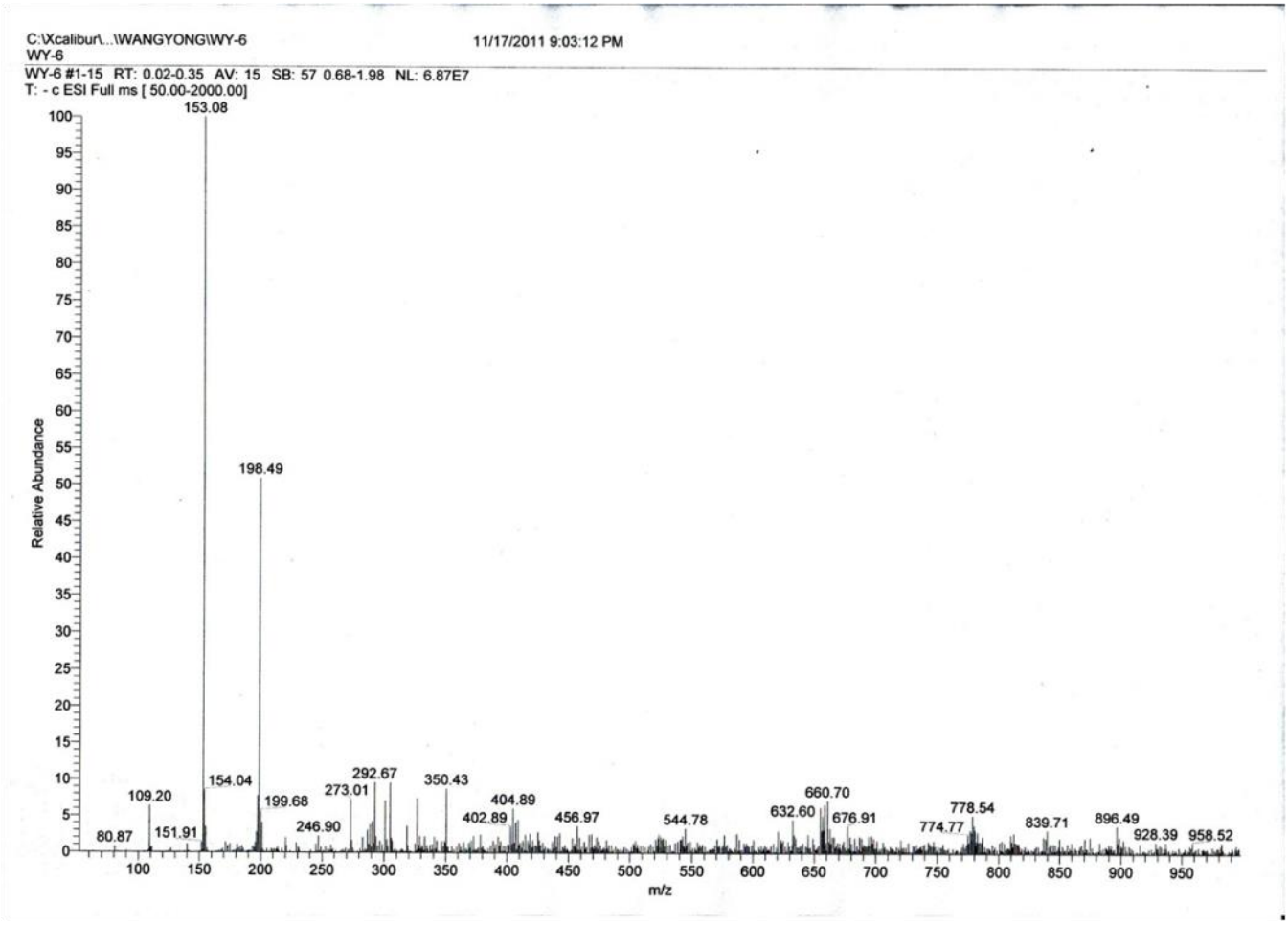

Figure S7. ESI-MS of freshly prepared 4-MBA solution in ethanol.

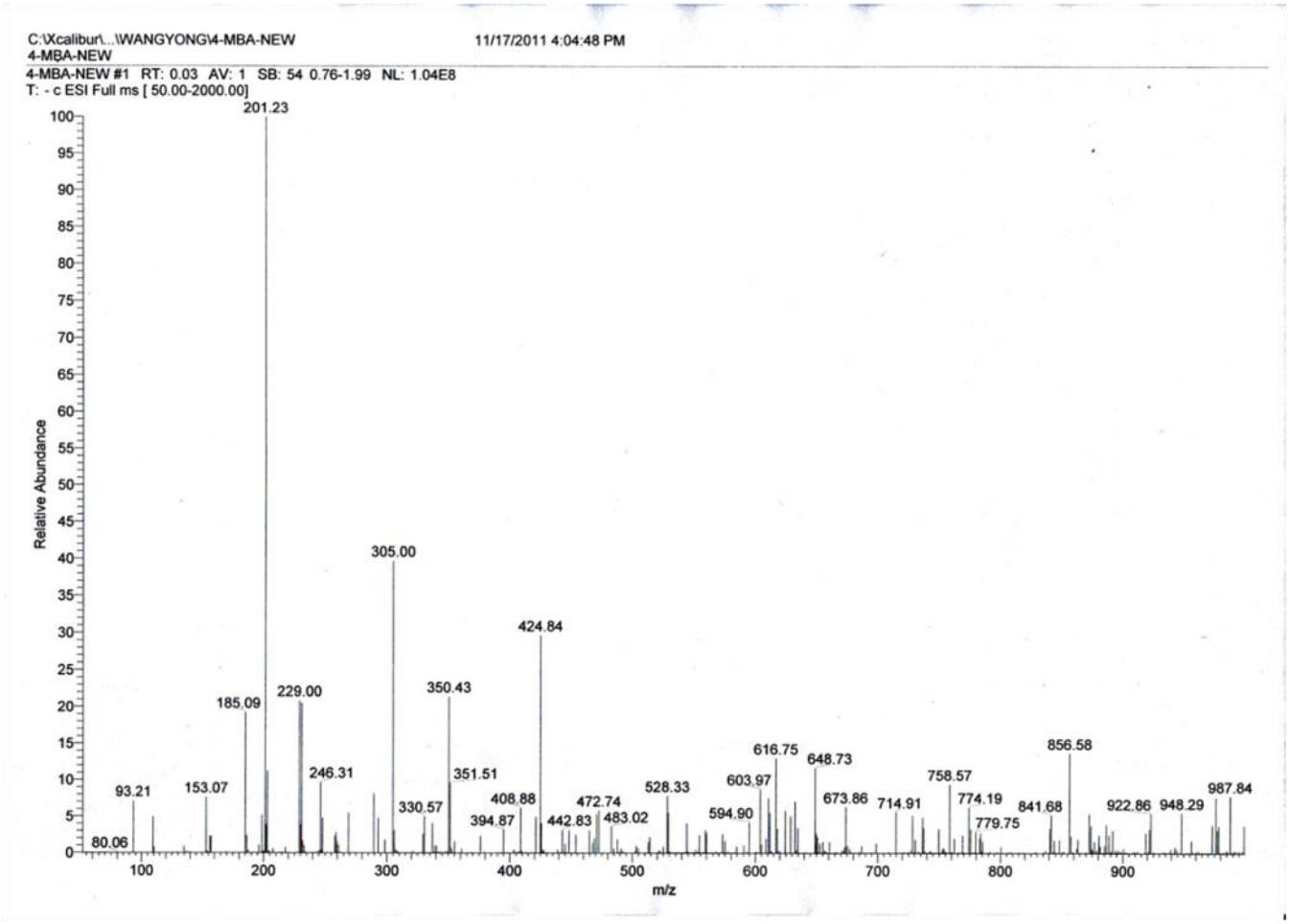

Figure S8. ESI-MS spectrum showing an ethanol solution of 4-MBA that was stored in sealed glass vial at room temperature for two weeks.

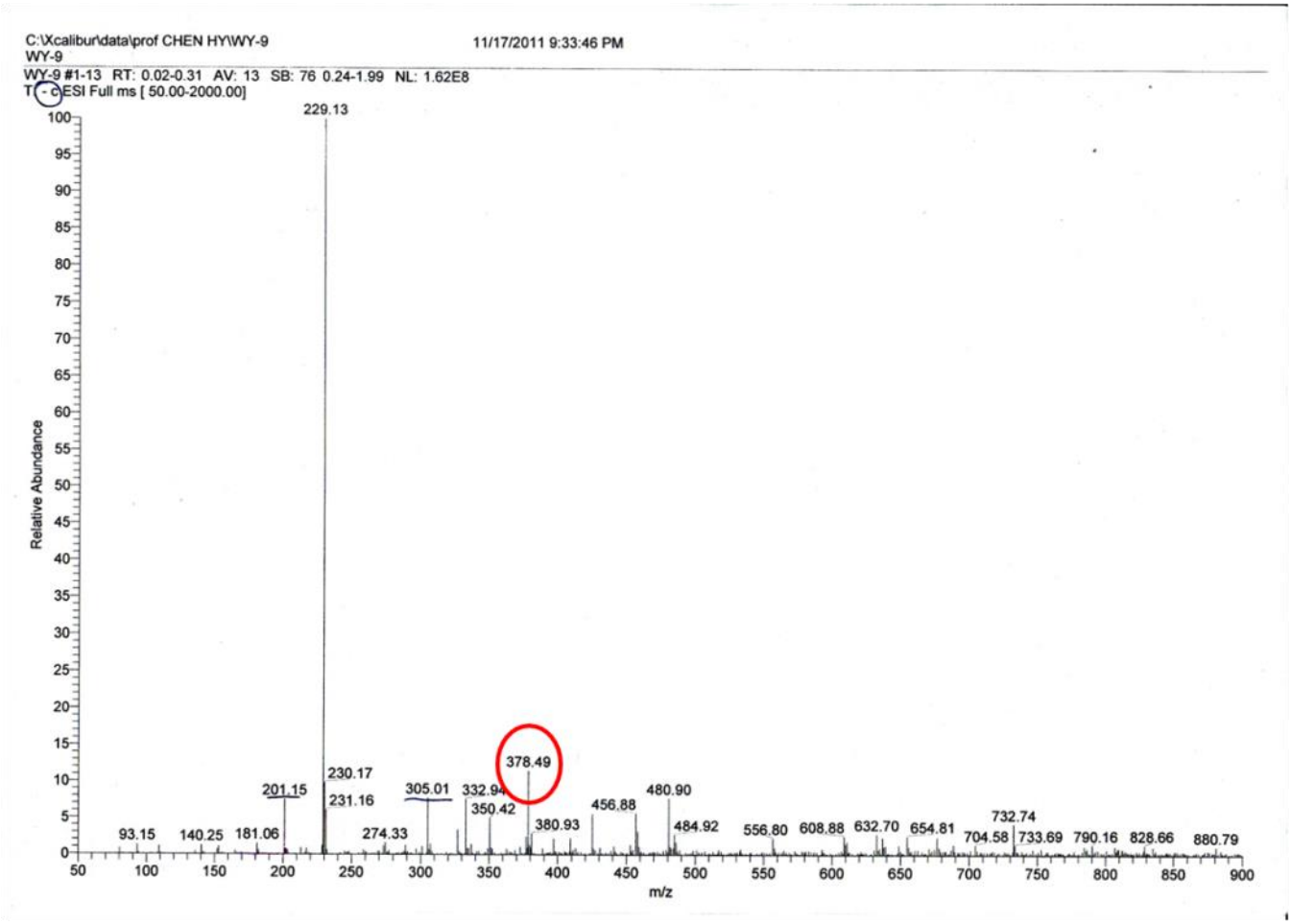

Figure S9. ESI-MS spectrum showing an ethanol solution of 4-MBA that was stored in sealed glass vial at room temperature for six months. In comparison to Figure S7 and S8, it is clear that 4-MBA underwent chemical changes when stored. The peaks circled in red are consistent with the ethyl ester derivatives of 4-MBA.

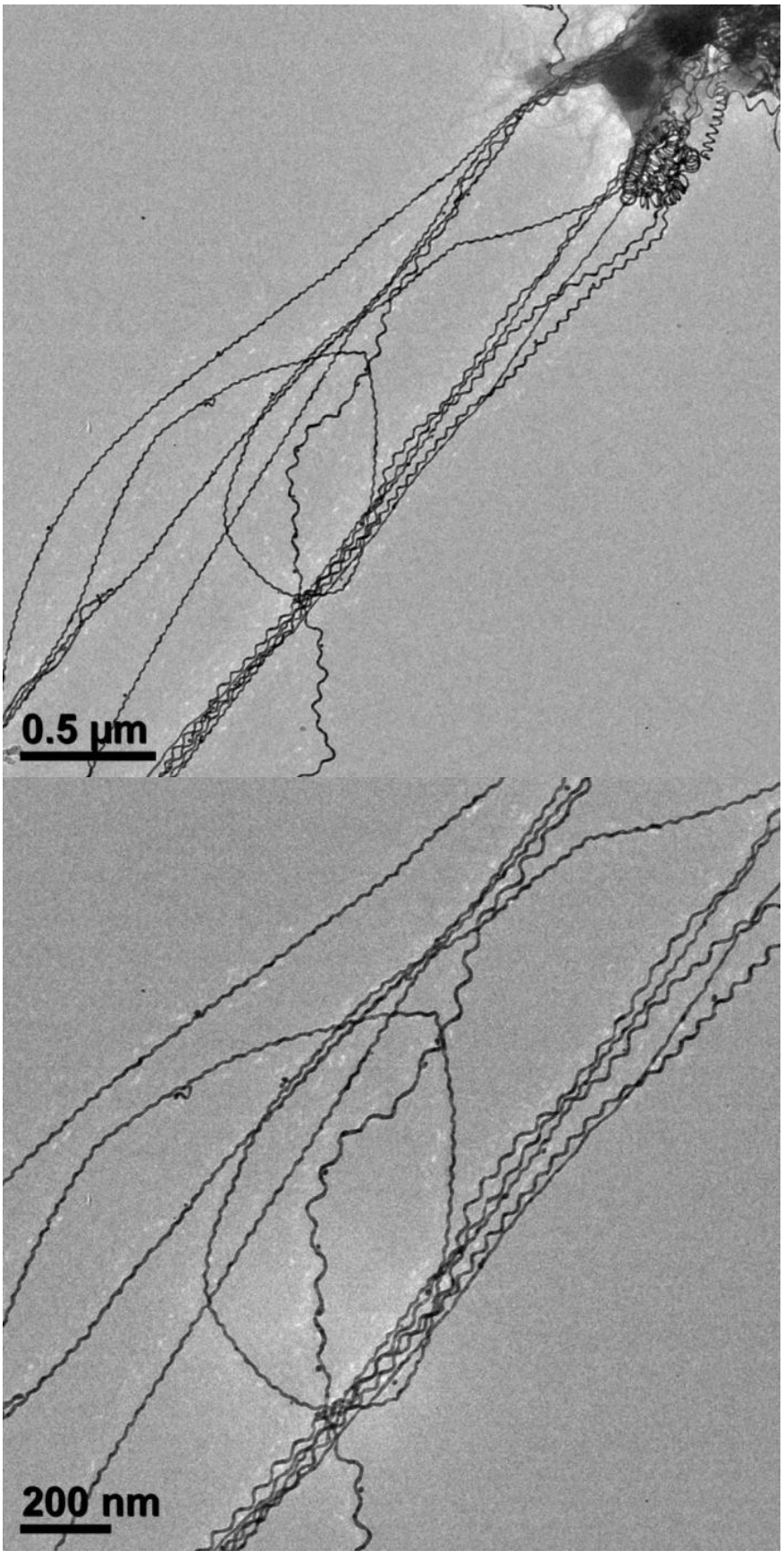

Figure S10. Large-area TEM images of the stretched helices with large pitch/width ratio, corresponding to Figure 1a.

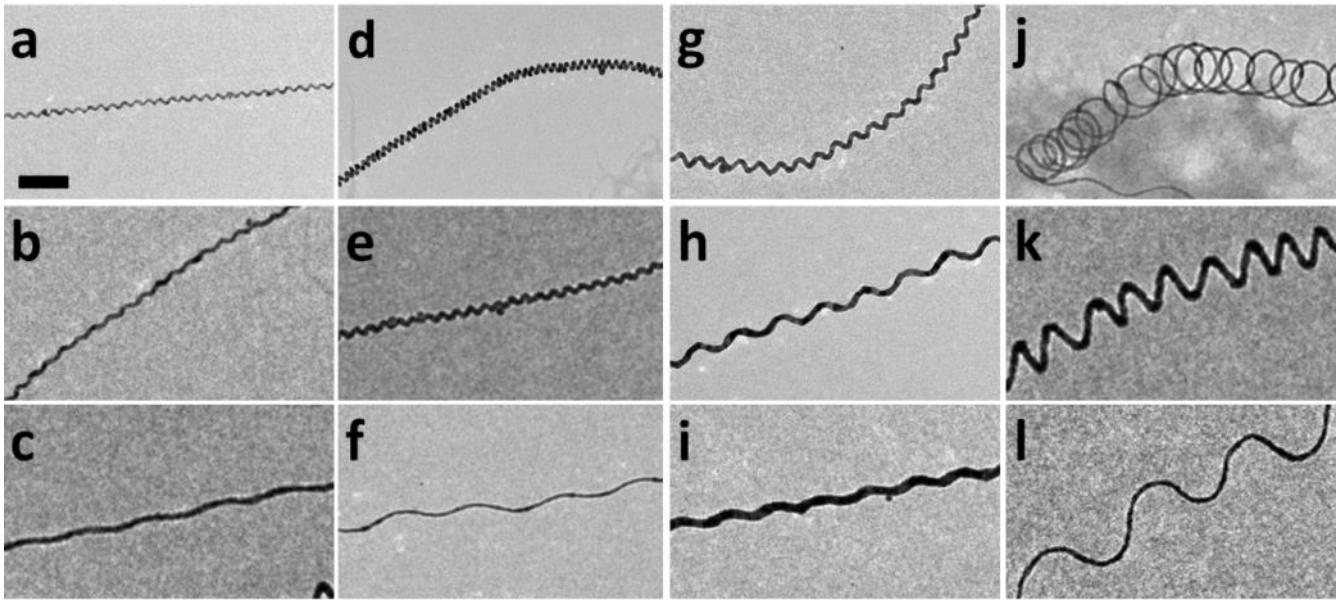

Figure S11. TEM images of the typical Au helices with various widths and pitches: (a-c) the widths are around 15 nm, and pitch lengths are from 25 nm to 150 nm; (d-f) the widths are around 25 nm, and pitch lengths are from 14 nm to 165 nm; (g-i) the widths are around 30 nm, and pitch lengths are from 40 nm to 110 nm; (j-l) the widths are around 95 nm, and pitch lengths are from several nm to 260 nm (same scale bar of 100 nm is shown).

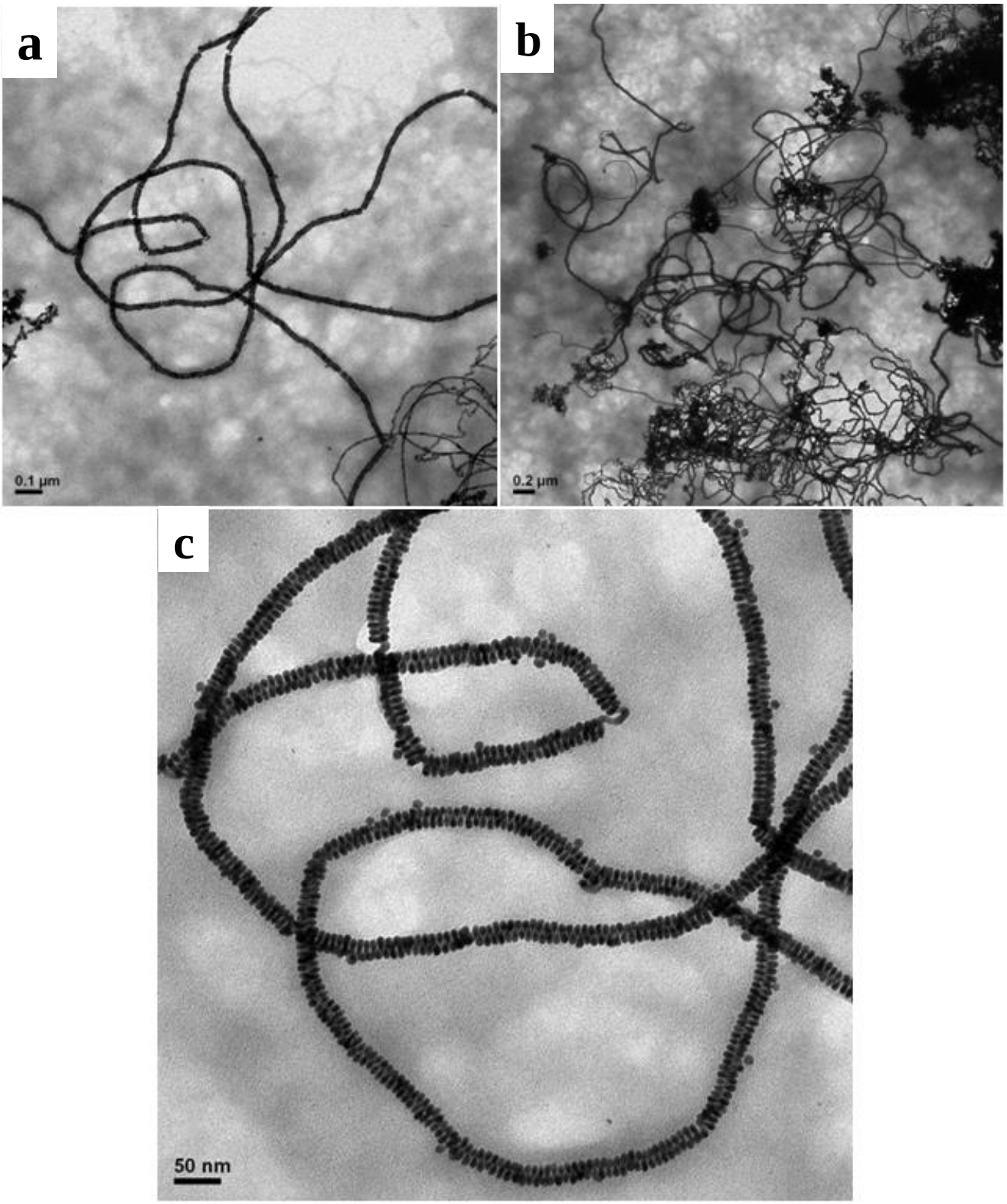

Figure S12. Large-area TEM image of the compact helices. The c panel shows an enlarged view of the central region of panel a. The aspect ratio (length/diameter over) of a is over 1,220 with over 1,200 pitches; the aspect ratio of b is over 22,300 with over 22,000 pitches.

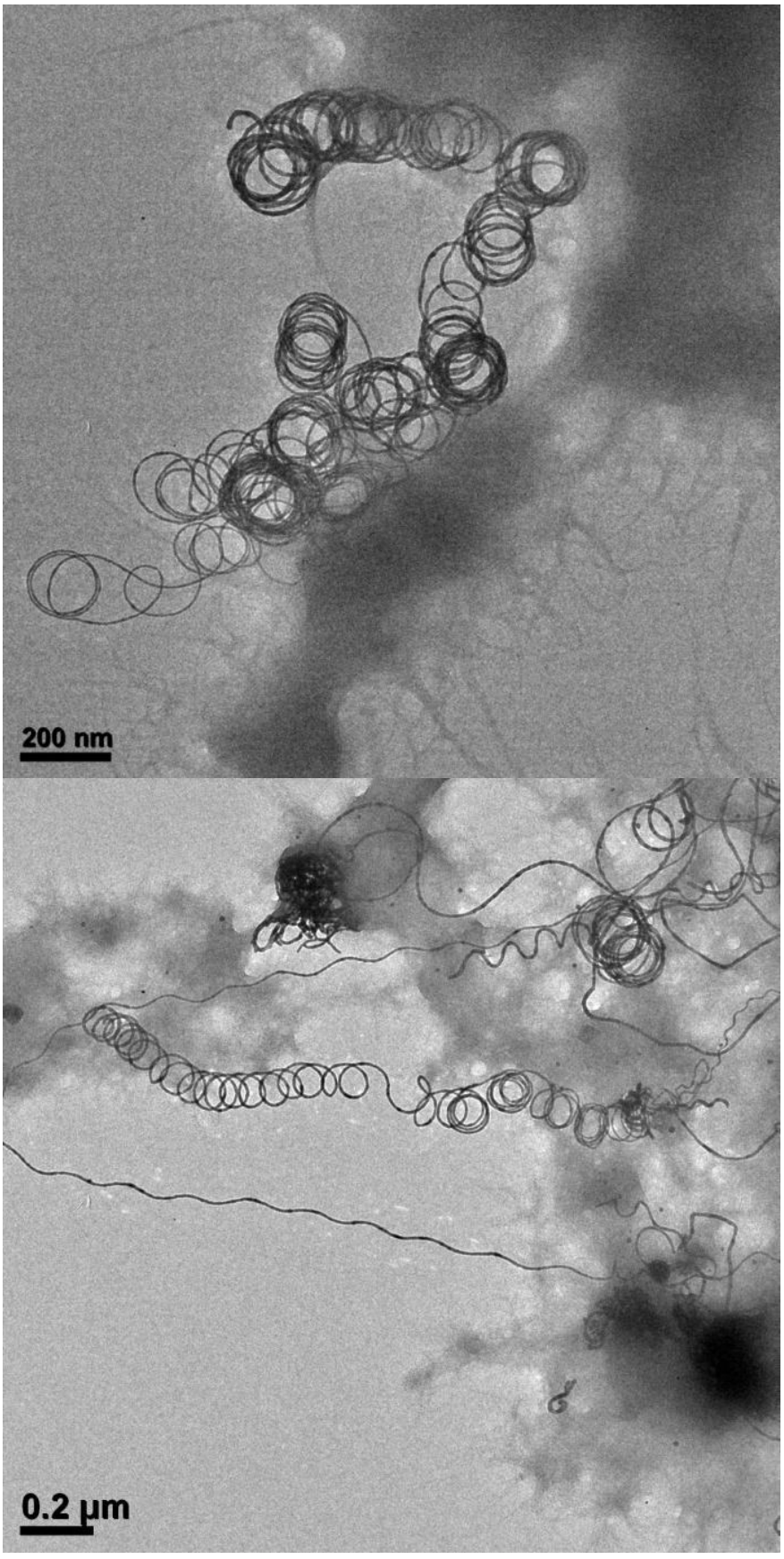

Figure S13. Large-area TEM images of the helices with small pitch/width ratio, corresponding to Figure 1c.

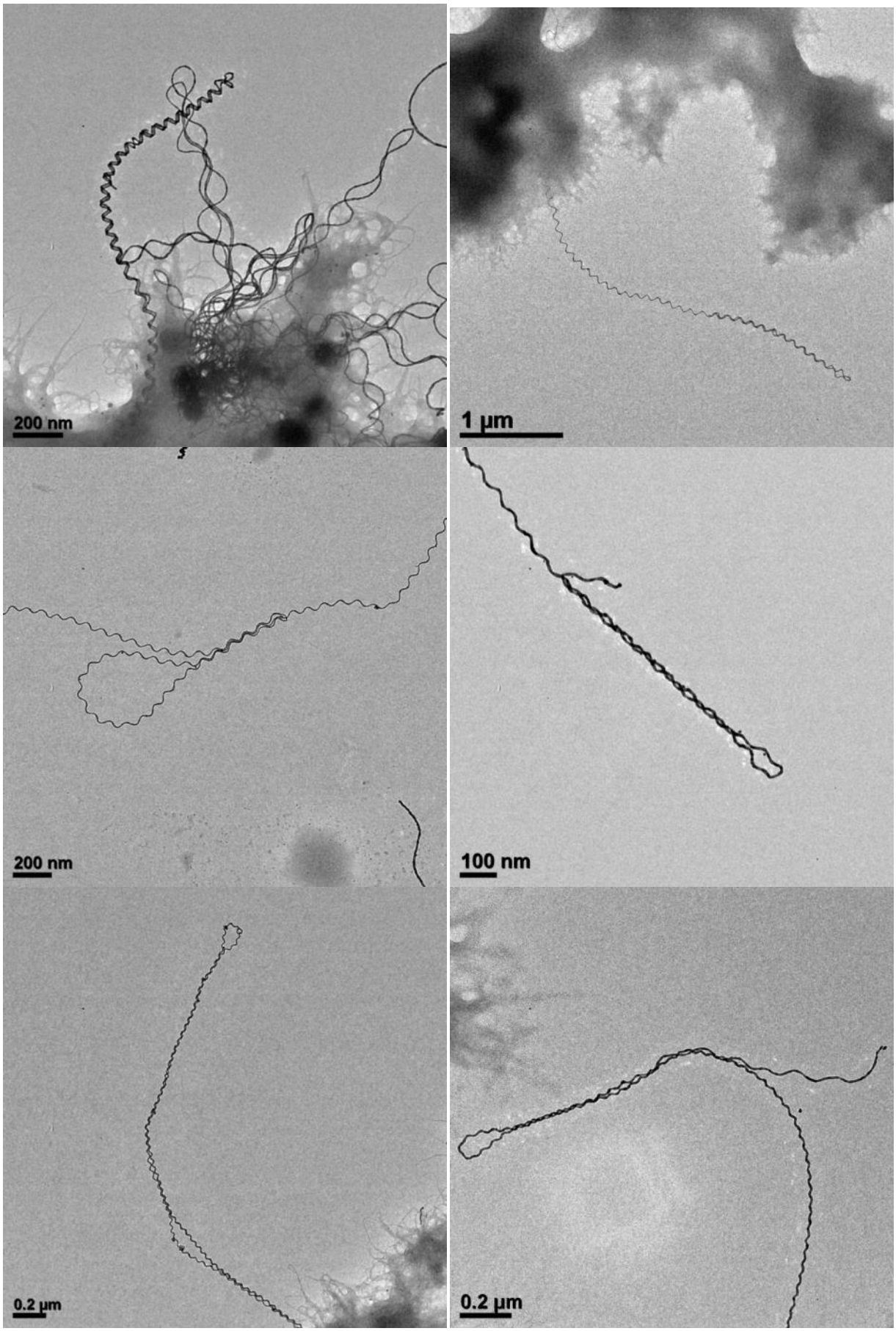

Figure S14. Large-area TEM image of the folded double helices, corresponding to Figure 1d and e.

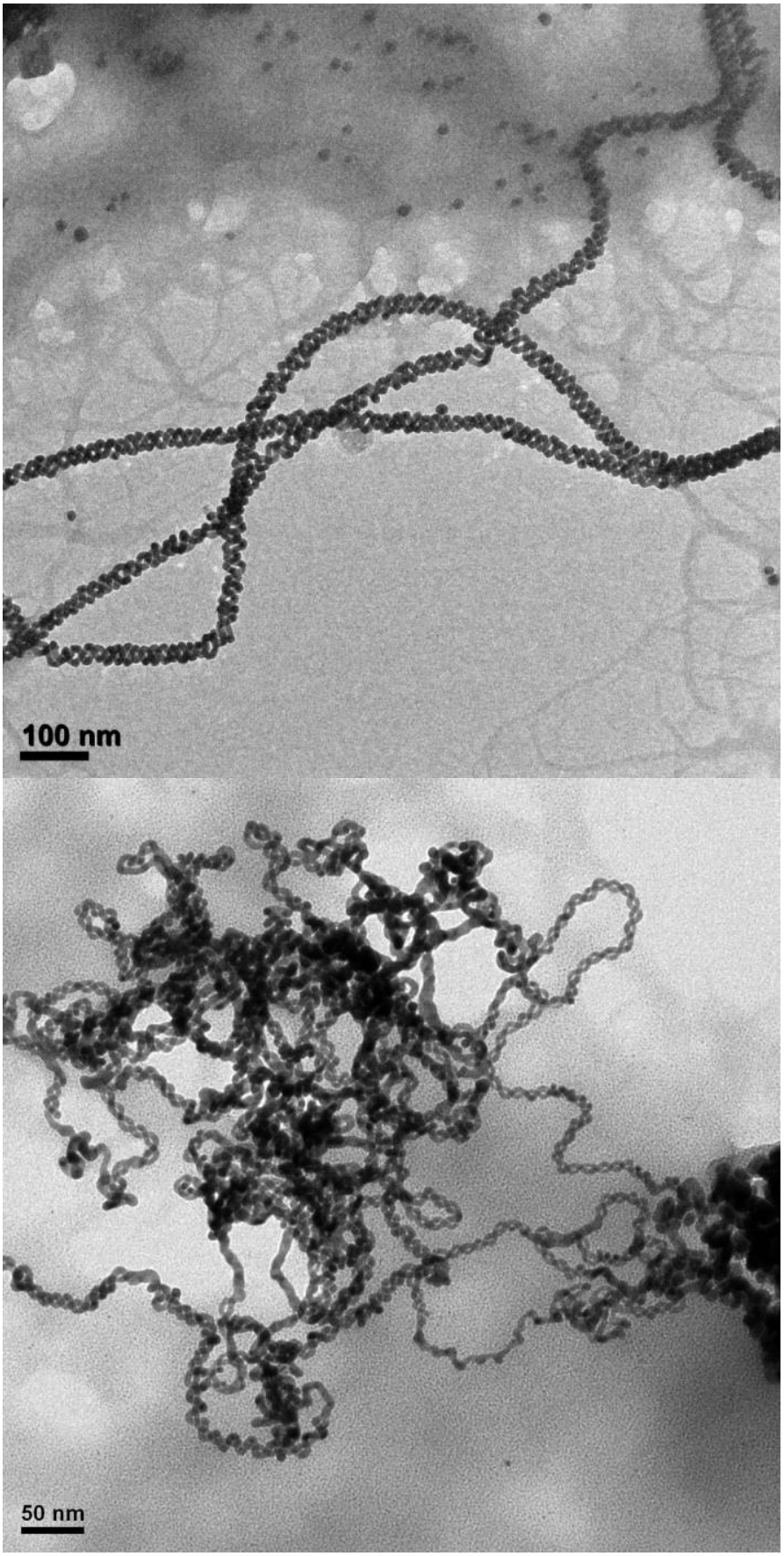

Figure S15. Large-area TEM image of the intertwined double helices of equal pitches, corresponding to Figure 1g.

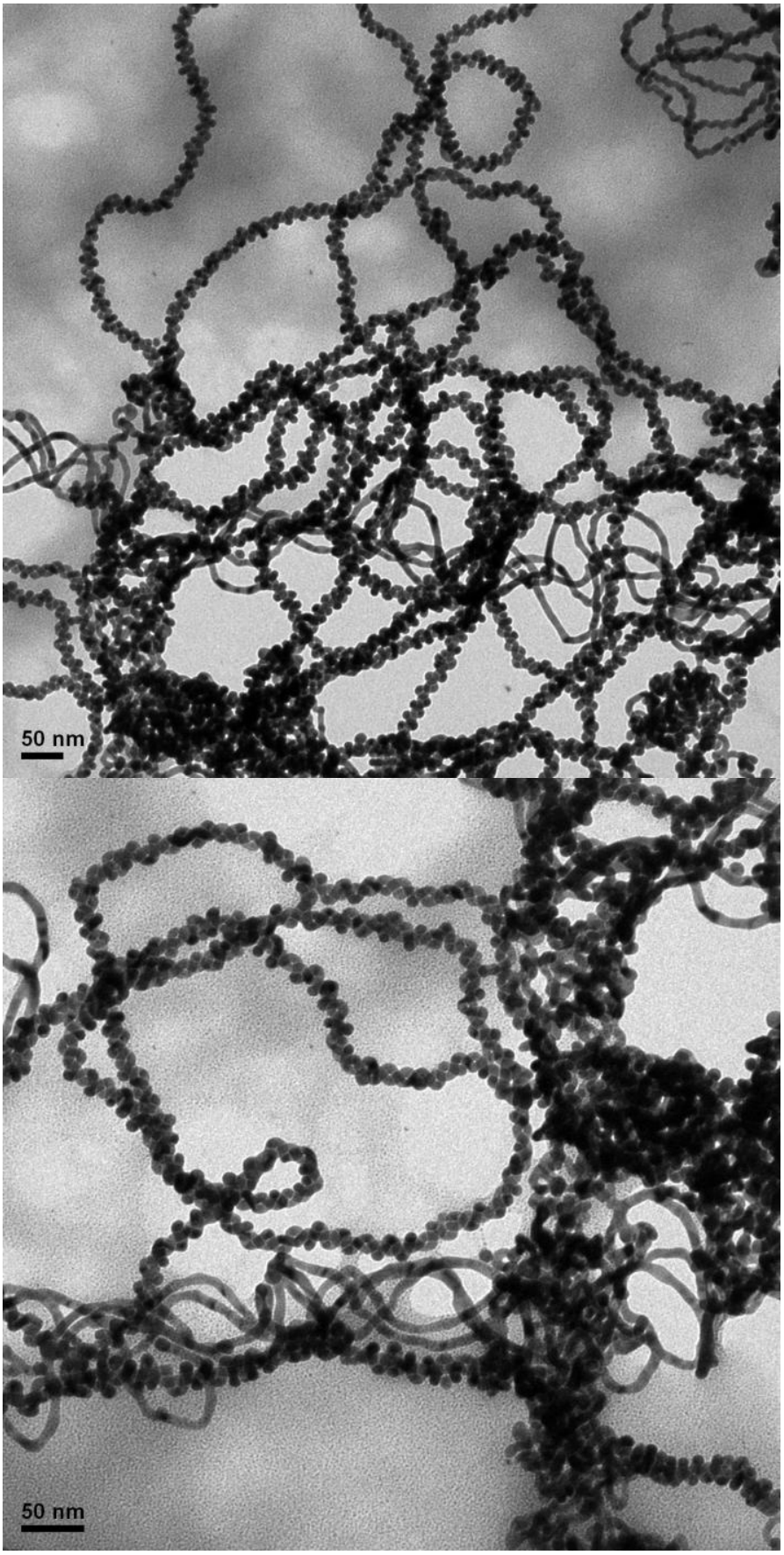

Figure S16. Large-area TEM image of the intertwined double helices of different pitches. One of the strands is even straight, corresponding to Figure 1h.

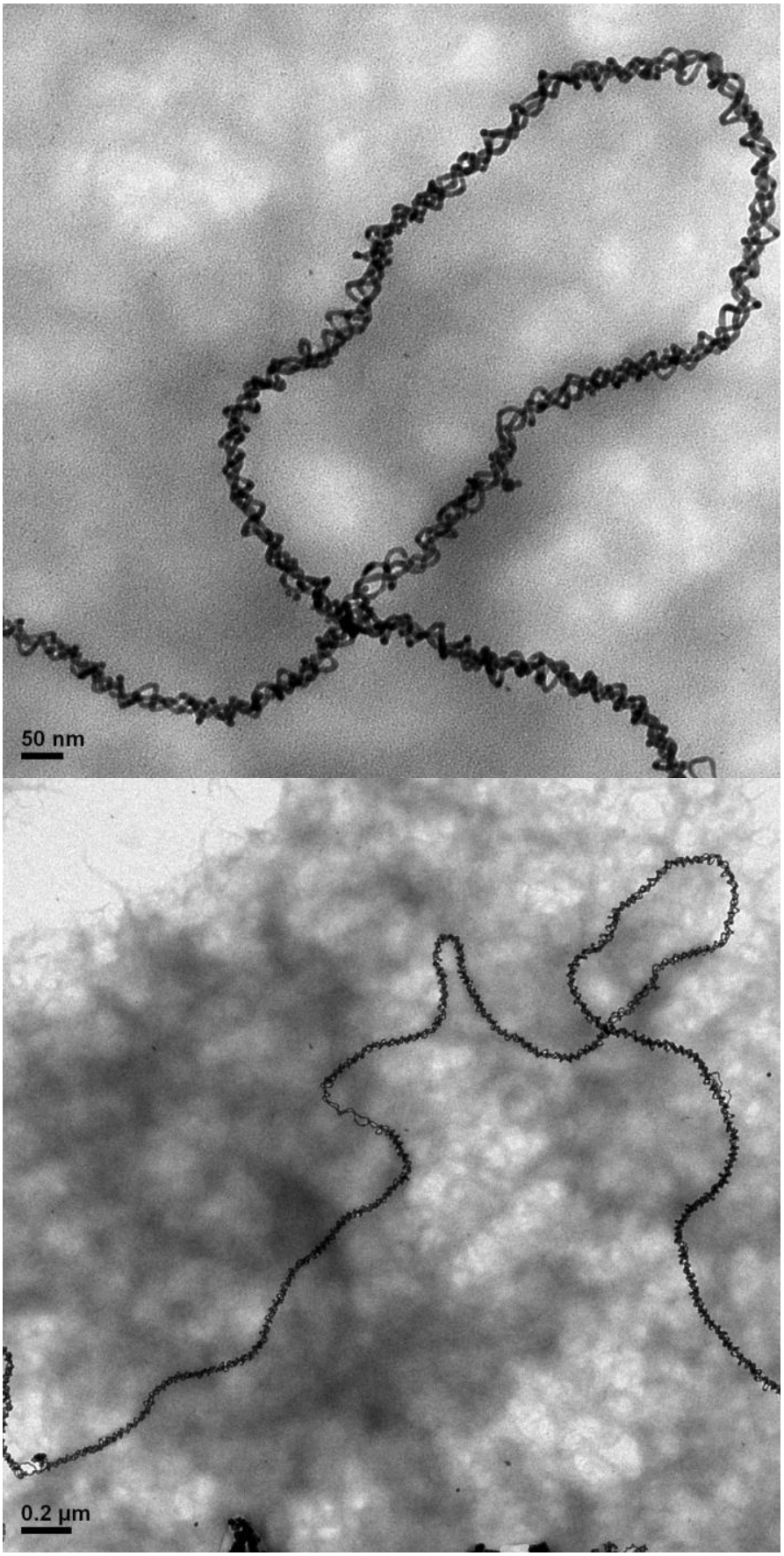

Figure S17. Large-area TEM image of the triple-strand helices of different pitches, corresponding to Figure 1i.

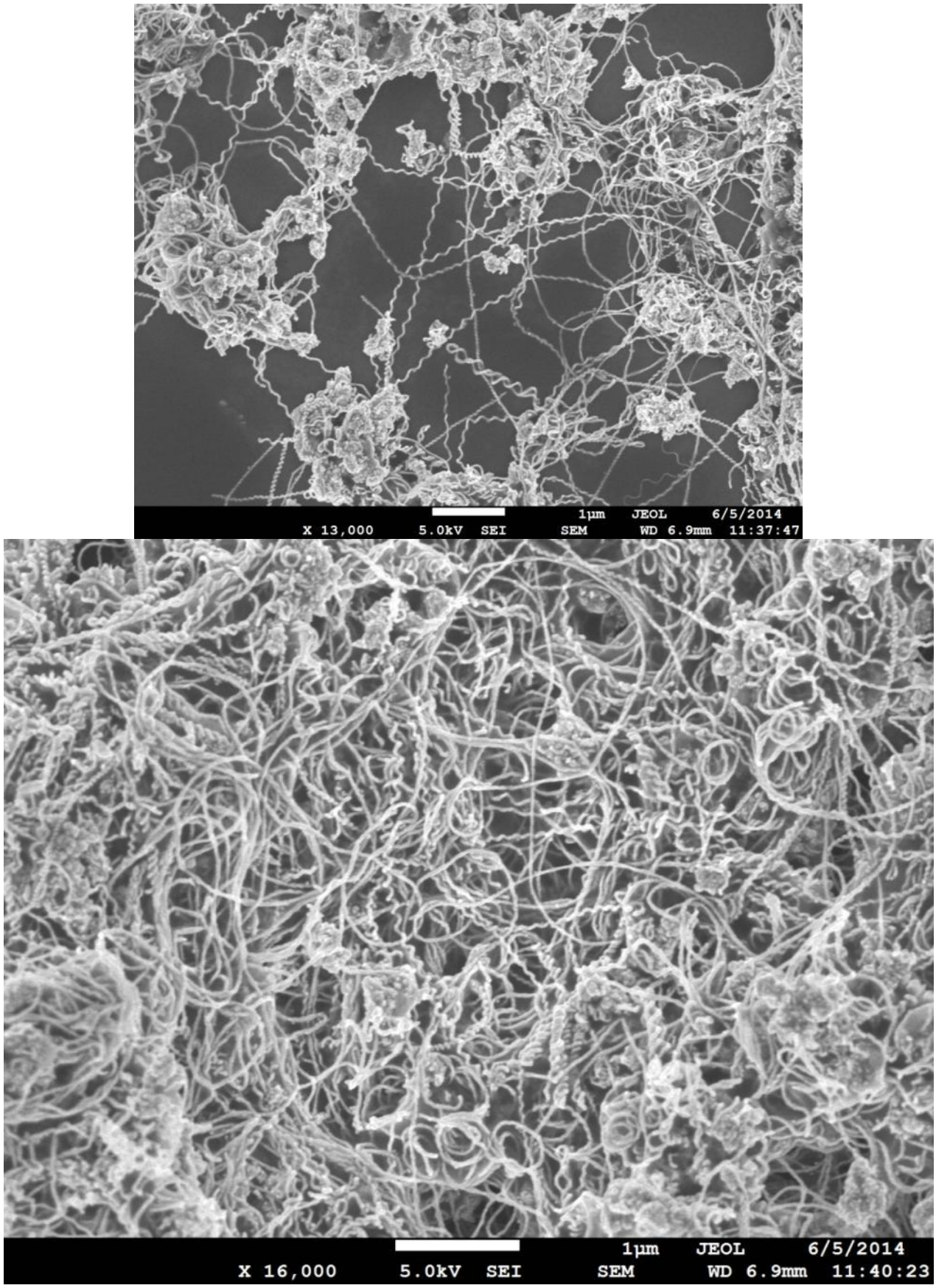

Figure S18. Large-area SEM image of the helices of different types, corresponding to Figure 2a.

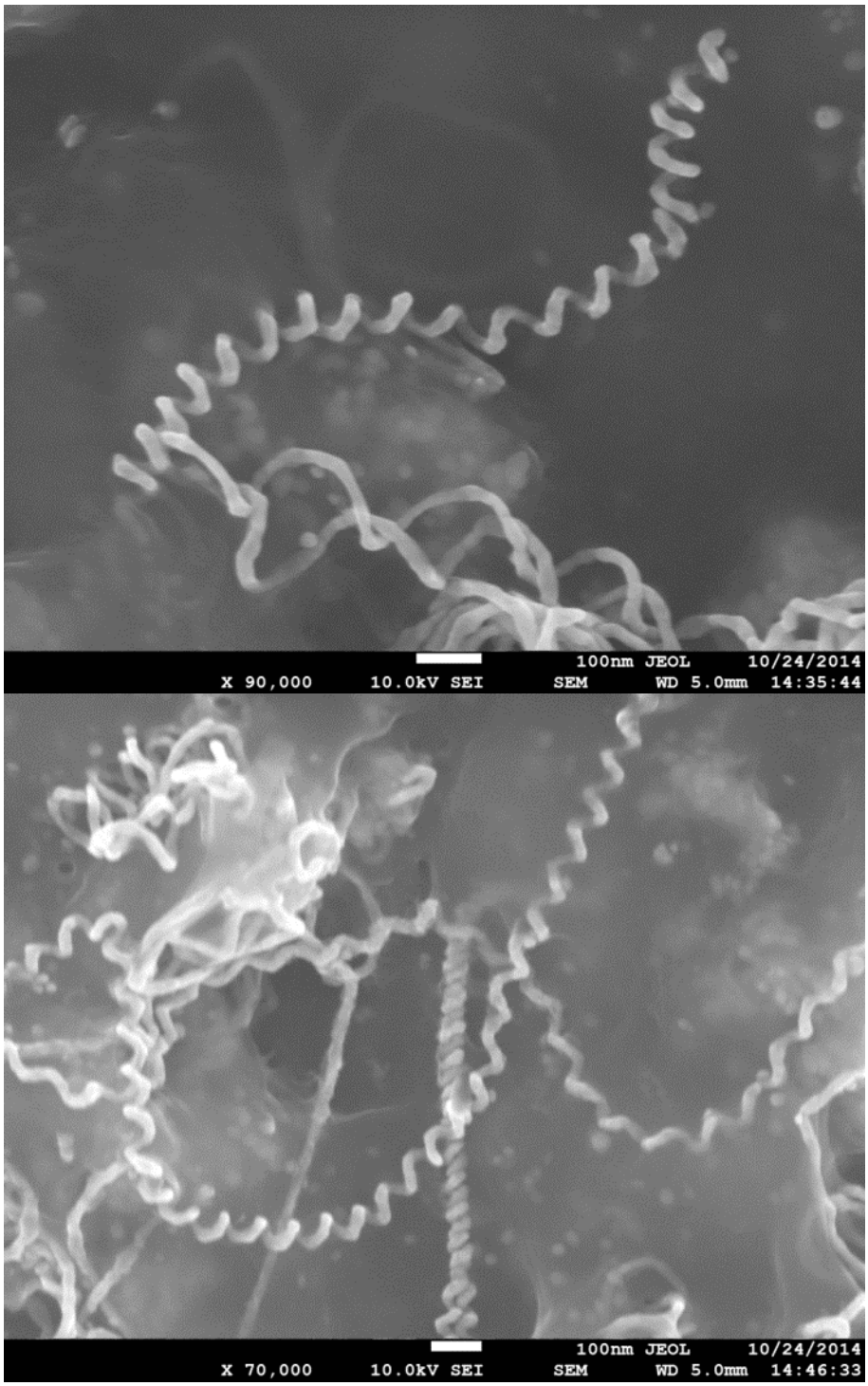

Figure S19. Large-area SEM images of the left-handed helices, corresponding to Figure 2d.

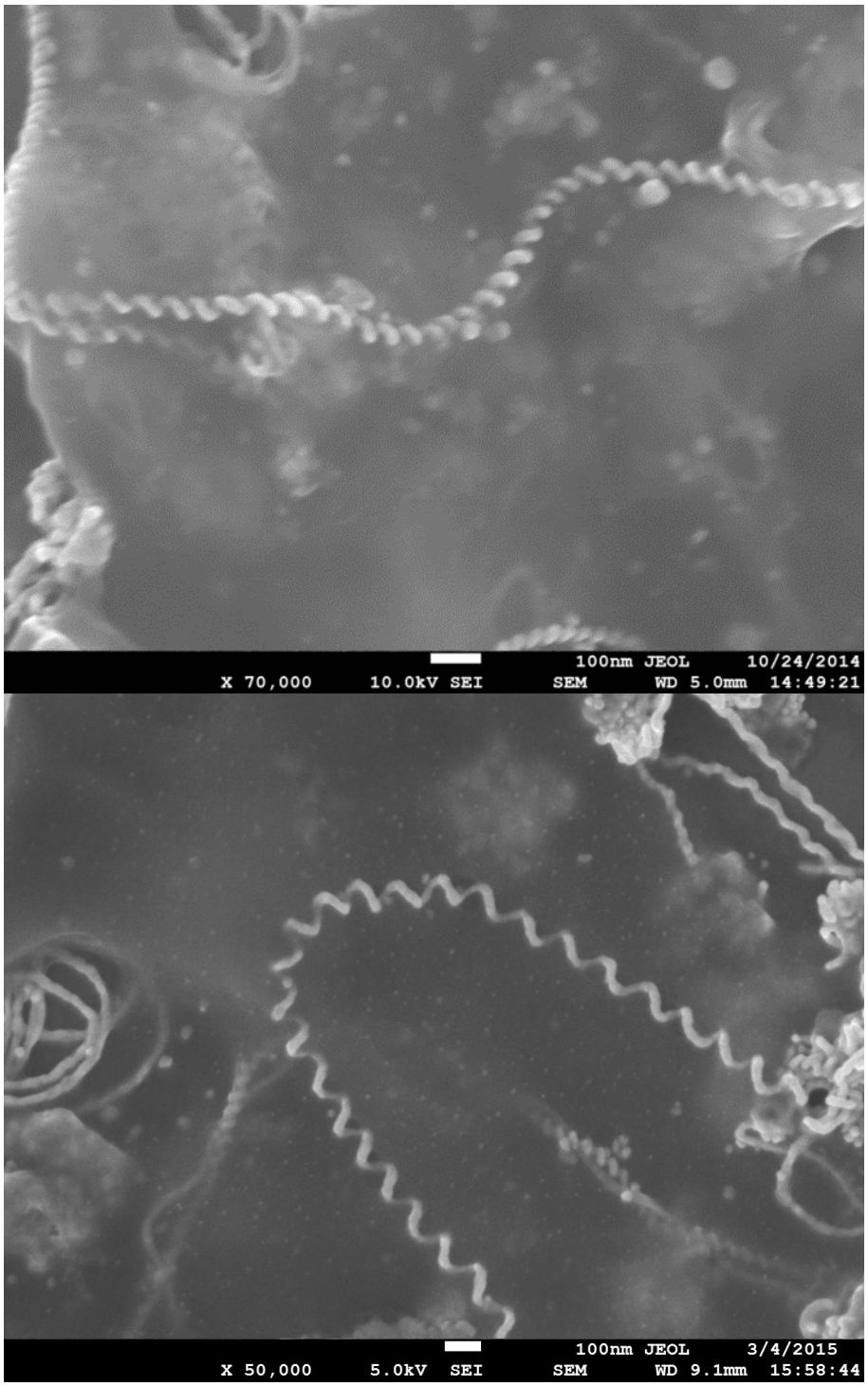

Figure S20. Large-area SEM images of the right-handed helices, corresponding to Figure 2e.

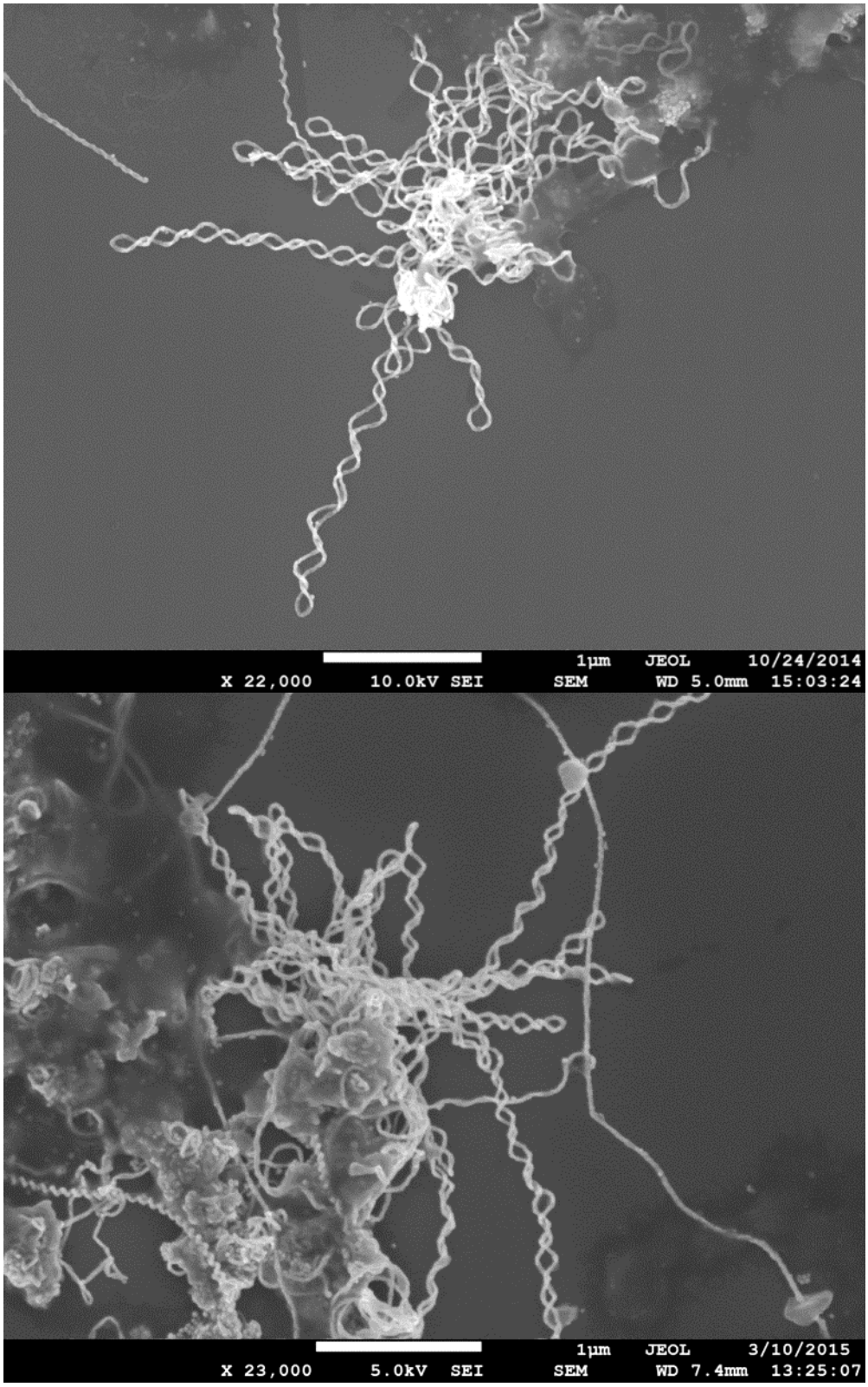

Figure S21. Large-area SEM images of the clusters of double helices with multiple left- and right-handed U-turn ends, corresponding to Figure 2f.

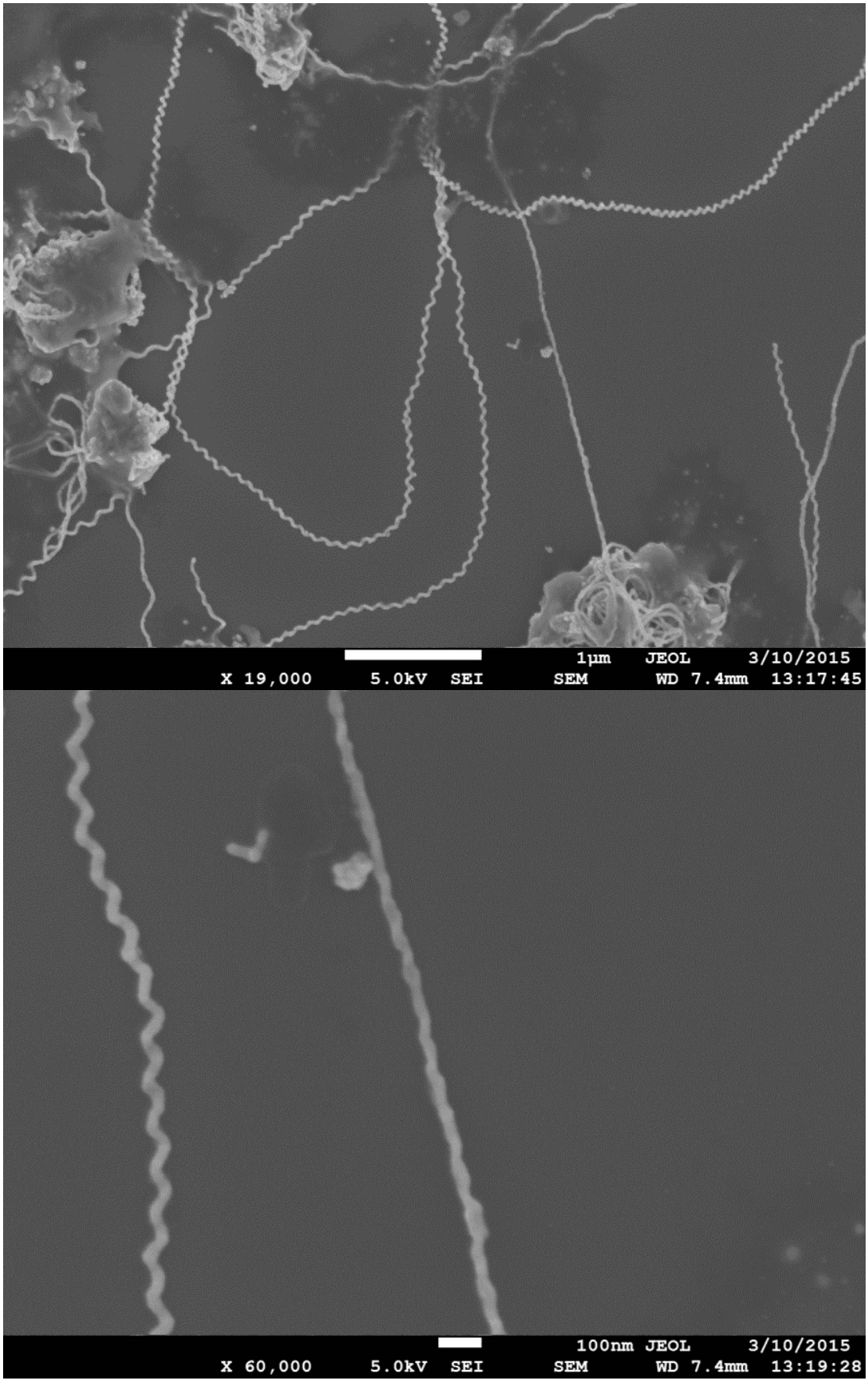

Figure S22. Large SEM images of the stretched helices with large and small widths, corresponding to Figure 2g.

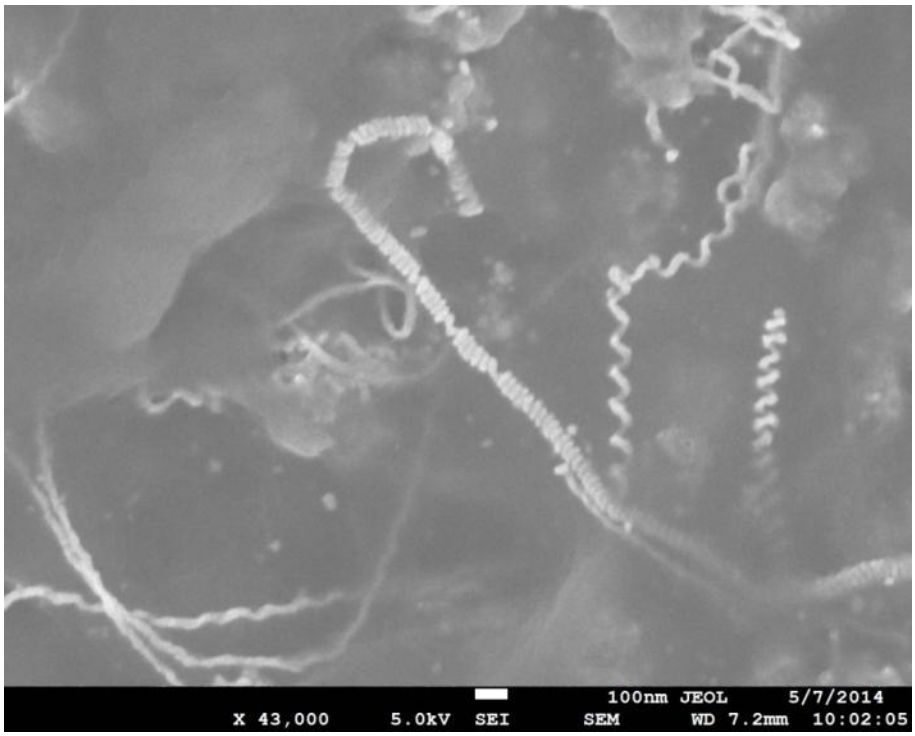

Figure S23. Large SEM images of the compact helices, corresponding to Figure 2h.

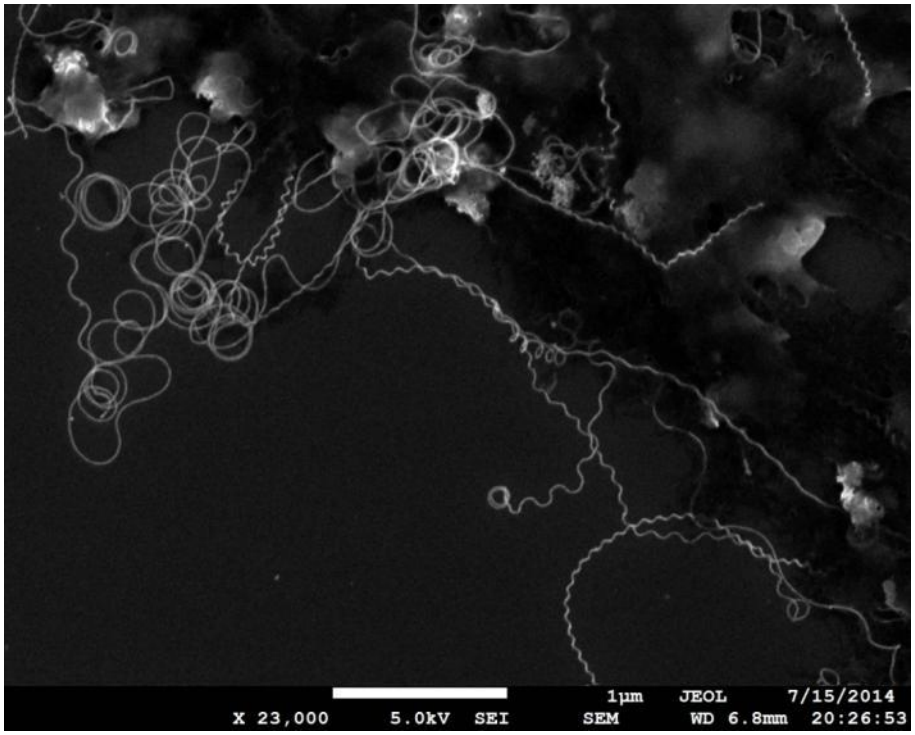

Figure S24. Large SEM images of the helices with small pitch/width ratio, corresponding to Figure 2i.

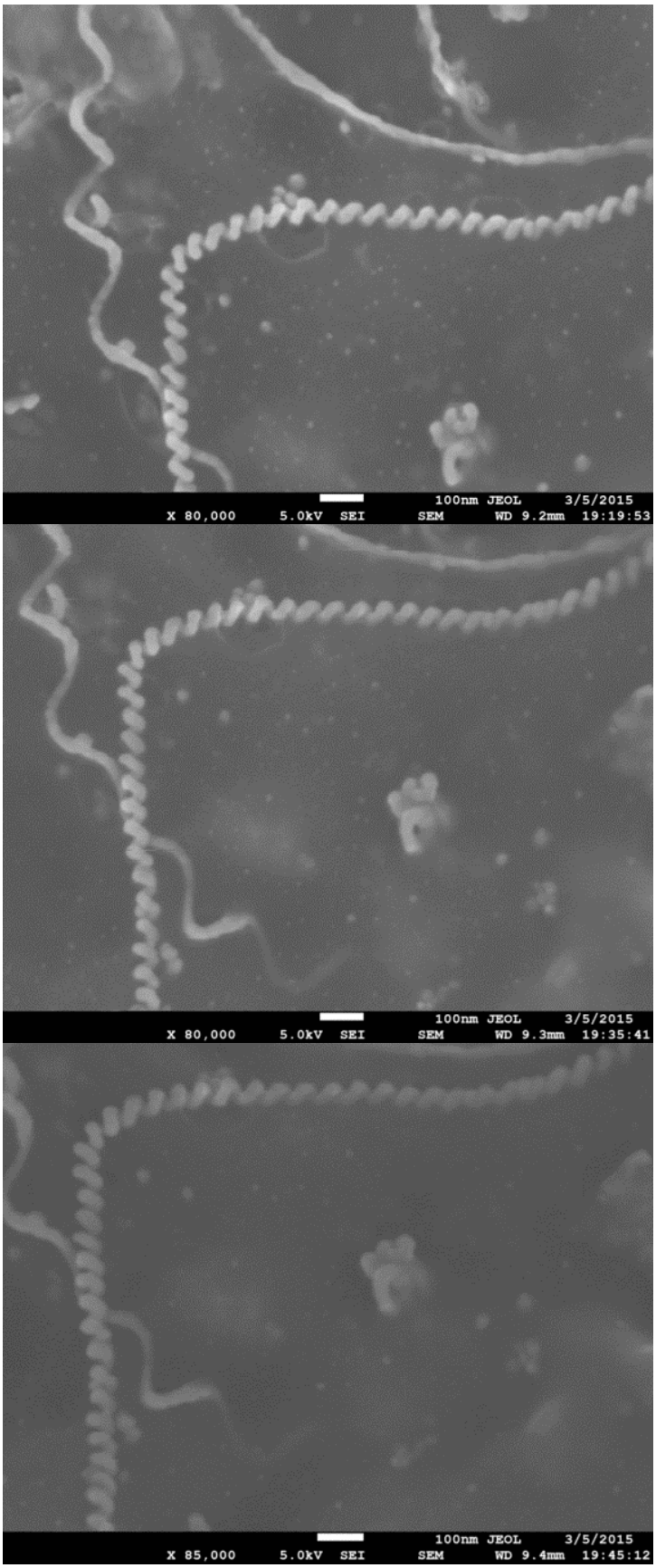

Figure S25. Large SEM images of the tilting study of a typical left-handed helix. The sample stage was not tilted, tilted by 25^{o}, and 40^{o} from top to bottom, respectively. These are the original images as shown in Figure 3a-c.

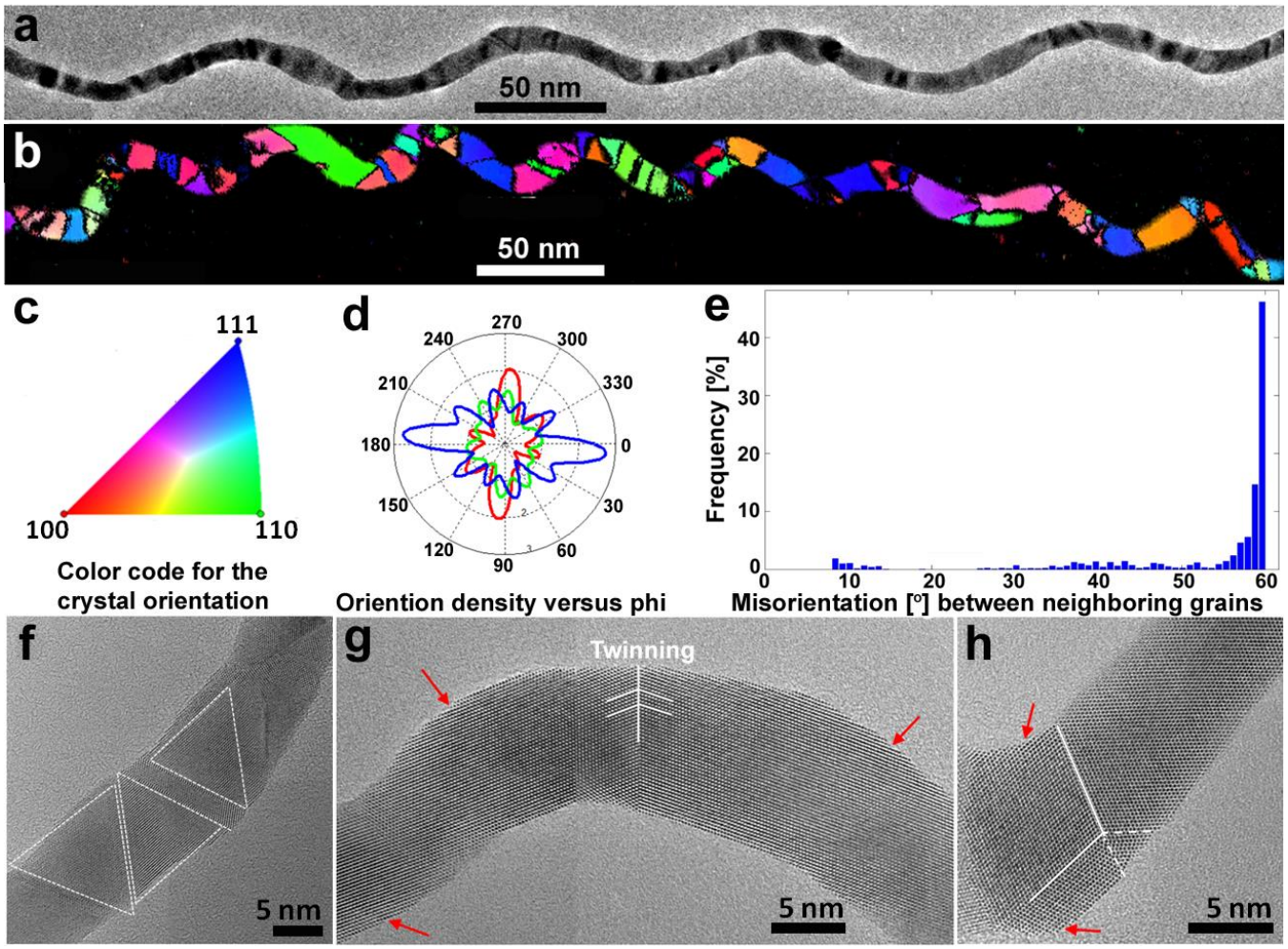

Figure S26. Enlarged Figure 4 in the main text.

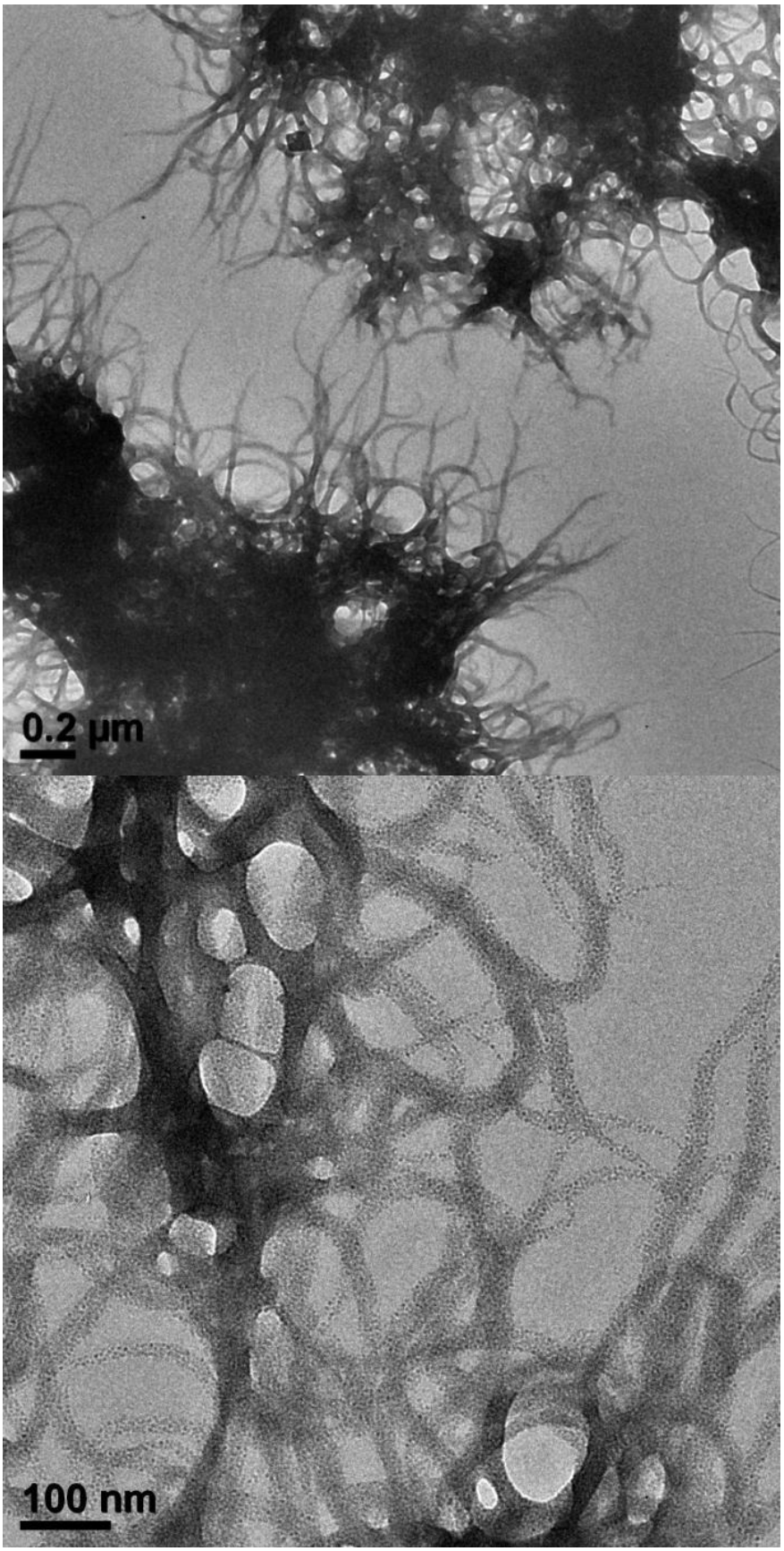

Figure S27. Floccules formed when the concentration of **1** was above 0.3 mM (top panel); these floccules can changes to lots of small nanoparticles once large dose of electron beam was applied (bottom panel).

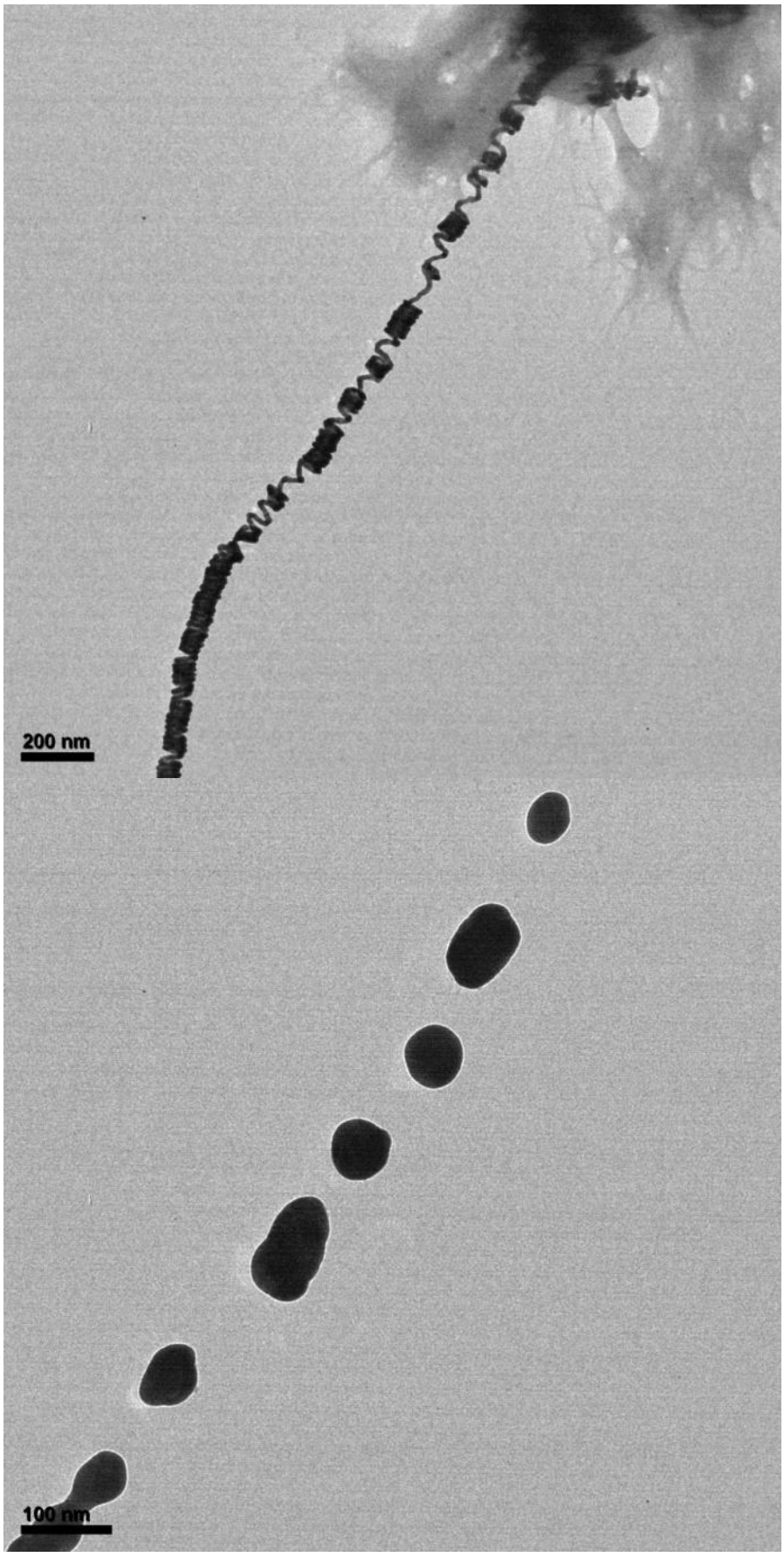

Figure S28. TEM images of gold helices under large dose of electron beam, showing a helix before (top panel) and after (bottom panel) the electron irradiation.

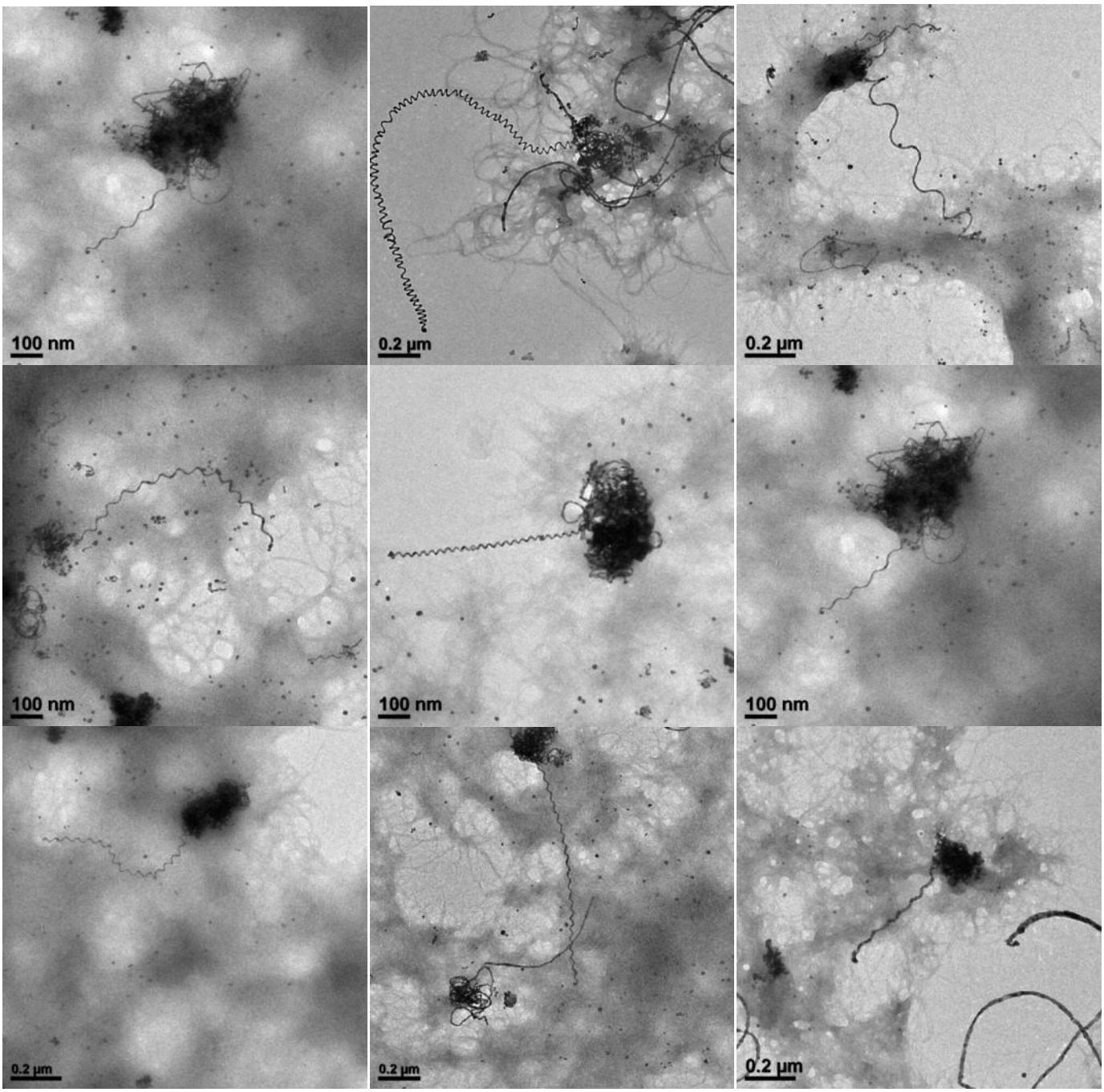

Figure S29. TEM images of some short helices extending out from "nests" made of nanowires.

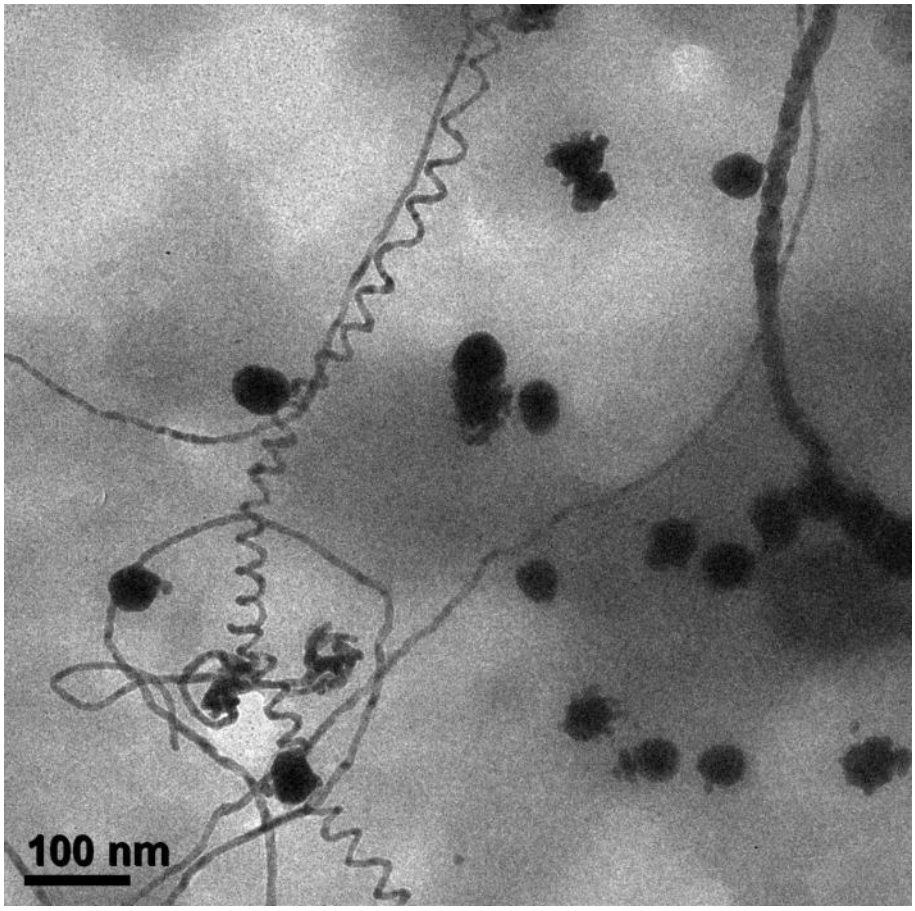

Figure S30. Enlarged TEM image of the control experiment where 30 nm Au nanoparticles were introduced as seeds in the growth solution but no helix was grown on them.